Evaluation of the collapsing thick-walled cylinder technique for shear-band spacing

Q. Xue, V.F. Nesterenko, M.A. Meyers*

Department of Mechanical and Aerospace Engineering, University of California, Mail Code 0411 9500 Gilman Drive, San Diego, La Jolla, CA 92093, USA

Abstract

The thick-walled cylinder (TWC) technique was successfully used to investigate the shear-band patterning in AISI 304 stainless steel. Several factors that may influence the shear-band distribution and spacing in the TWC configuration were examined. The role of machining, annealing, and shrink fitting, as well as the variation of the shear-band distribution along the longitudinal axis of the cylindrical specimen were evaluated. Experimental results indicate that the machined surface at the internal boundary of the cylindrical specimen, where shear bands initiate, provides a strain-hardened layer that significantly changes the condition for their initiation. Specimens with such a layer have a higher density of bands with a smaller spacing, in comparison with those without a work-hardened layer. The nature of contact interface in the cylindrical specimen assembly, either causing a clearance that changes the initial loading conditions or introducing a pre-strained layer with shrink-fitting technique, does not influence the spacing of shear bands, but does affect the evolution and development of multiple shear bands at the initial stage. The distribution of shear bands along the cylinder has a constant spacing but the maximum lengths of bands are sensitive to the position. The collapse process of the cylindrical specimen was simulated by using the RAVEN hydrocode. The deformation, temperature, and velocity histories during the cylinder collapse were calculated. The calculated results are in good agreement with the previous experimental data.
© 2002 Elsevier Science Ltd. All rights reserved.

Keywords: Thick-walled cylinder; Shear bands; Patterning

---

*Corresponding author. Tel.: +1-858-534-4719; fax: +1-858-534-5698.
E-mail address: mameyers@mae.ucsd.edu (M.A. Meyers).

1. Introduction

Multiple shear bands have been found in various types of dynamic experimental processes such as ballistic impact, projectile penetration, explosion fragmentation, machining, etc. [1–4]. The properties of the assemblies of shear bands determine to a large extent the overall evolution of failure. The spatial distribution and number of multiple shear bands depend on the loading conditions, interactions among them, as well as material properties. A periodic distribution of shear bands often constructs a spatial pattern described by characteristic spacing. The spacing of shear bands in a 1-D geometry has been analyzed theoretically, assuming different mechanisms [5–7]. However, there are very limited experimental studies focusing on multiple shear bands and their spatial distribution. One of the major difficulties is the lack of efficient techniques to provide a controllable, uniform, and reproducible loading of the samples, allowing for the development of multiple shear bands.

The development of shear bands in most cases requires an unstable condition. A single band may develop immediately after the instability of deformation and arrest the initiation of other localization zones, as in a torsional [8,9] or shear (hat-shaped [10–13]) Hopkinson bar experiments. Multiple shear bands, on the other hand, develop from an evolving loading condition. For example, multiple shear bands are often found in ballistic impact, but loading conditions at the bottom and lateral wall of a crater are quite different. Backman and Finnegan [14] first compared the shear-band pattern in ballistic impact with the theoretical slip-line as a result of local surface loading. The traces of shear bands are incredibly similar to one of the families of slip lines. Grebe et al. [4] measured the numbers of shear bands generated in Ti and Ti6Al4V in ballistic impact and observed two differences: (a) Ti exhibited a larger number of shear bands than Ti6Al4V; (b) the shear bands propagated more extensively along the rolling direction than perpendicular to it. Wittman and Meyers [15–17] compared the trajectories of bands in ballistic impact for steel and observed their characteristic spacing as well as their spiral shape corresponding to the slip-field analysis. This strongly suggests, and is indeed commonly accepted, that shear bands develop along the paths of the maximum shear stress. The simple shear condition is most frequently used to investigate shear localization under controlled strain. Although the loading condition is quite simple, multiple shear bands rarely occur under simple shear experiments because of the relatively short gauge section in comparison with the expected shear-band spacing. Thus, a single shear band dominates the experiment. Nevertheless, two shear band structures were observed under simple shear in steels [18,19] and in Ti-6Al-4V alloy [20].

There are very few methods that can provide a well-controlled condition for the development of multiple shear bands. The contained exploding cylinder (CEC) is a group of effective techniques to examine shear localization. Multiple bands were found to initiate and propagate outward at the internal boundary of the explosively expanding thin-walled cylindrical specimens [21–23]. The initial motivation of such an experimental configuration was related to fragmentation problems of spherical and/or cylindrical shells. Adiabatic shear bands were found to give the paths of fracture in these experiments and finally to lead to fragmentation. These shear-band patterns on the cylinder specimens usually follow a group of spiral paths and their initial orientation is roughly 45° to both the radial and circumferential directions. However, this loading configuration produces a tangential tensile stress state on the circumference of the cylinder. This tensile stress leads to multiple cracking along these developed shear bands. Nesterenko et al. [24–33] proposed

an imploding method, based on the collapse of a thick-walled cylindrical specimen. This method is often called thick-walled cylinder (TWC) technique. The thick-wall geometry of the specimen is of principal importance because it eliminates the geometrical instabilities that are typical in the collapse of thin-walled cylinders. Materials resistant to shear localization (for example, copper, which work hardens substantially) were selected to make driving and stopping tubes to provide a controllable loading process. The schematic configuration of this device is shown in Fig. 1. The main differences between the CEC and TWC methods are that the latter generates compressive stresses in both radial and circumferential directions during the development of shear bands, while the former is characterized by tensile stresses in the circumferential direction during the expansion stage. Another difference is that, in TWC method, the explosively loaded surface is separated from the surface where shear bands are nucleated. High explosives (C-4 with the density of 1.65 g/cm^3 and detonation speed of about 7 km/s) are used in CEC method. The use of this type of explosive in the TWC geometry would result in a excessive melting in the center and fracture. That is why low-density industrial explosives (density of ~ 1.0 g/cm^3 and detonation speed of 3.5 km/s) are employed in the TWC method. Moreover, the geometrical parameters of the sample, driver tube, and explosive in TWC method are specially selected to ensure that no spalling occurs in the vicinity of the inside surface. The kinetic energy is primarily consumed by the collapse. This ensures that effects due to backward motion remain negligible. The large difference between detonation speed and velocity of collapse ensures a small angle between axis and the collapsing wall; the TWC method can be approximately considered as a simultaneous collapse with cylindrical symmetry. Using such a technique and its modified versions, Nesterenko et al. [29], Nesterenko [30], and Xue et al. [31,32] investigated large strain deformation and shear localization in porous reactive mixtures of powders (Mo, Ti, Nb with Si, Ti and graphite); in metals (stainless steel, Nb, copper (different grain sizes), CP Ti); in densified or pre-fractured ceramics (Al$_2$O$_3$ and SiC); and in polymers like Teflon. The TWC technique has revealed the patterning and spacing of multiple shear bands in these materials.
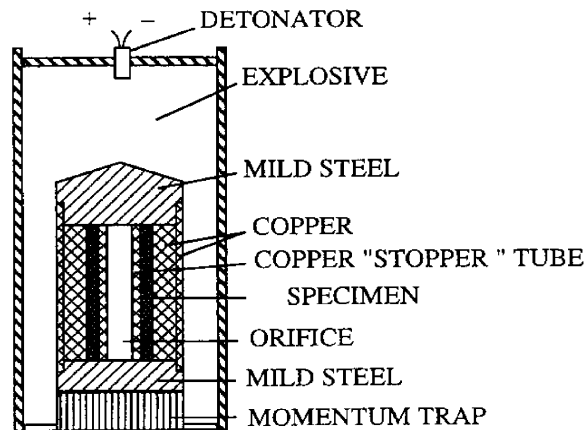
Fig. 1. Thick-walled cylinder (TWC) technique with imploding configuration. Notice that the explosive is outside (from [29]).

It was felt that some effects from the different geometrical or loading conditions, such as the configuration of the driving and stopping tubes, could affect the development of the shear-band pattern. Thus, the purpose of this research is to investigate the role of experimental parameters on the characteristics and spacing of multiple shear bands. These may include the quality of machined surface and the existence of a gap between copper stopper and tested cylinder specimen. Possible dependence of the shear-band patterns along the cylinder specimen was also addressed especially due to the fact that there is a small axial angle of collapse carried by the inclined deformation wave [34]. The spatial distribution of multiple shear bands in the cylinder specimen was investigated and compared with previous predictions. The collapse process was simulated by using a Eulerian-based hydrocode Raven in order to obtain a good quantitative understanding of the collapse process.

2. TWC technique for the study of patterning of shear bands

2.1. TWC explosion technique

The TWC specimen is surrounded by the explosive axisymmetrically. Once the detonation is initiated on the top, the weak shock wave created from the explosion exerts a uniform pressure on the cylindrical assembly and drives the specimen to collapse inward. The detonation velocity of the selected explosive is approximately $D = 4000$ m/s and the density of the explosive is 0.9 g/cm^3. The velocity u_w of the inner wall of the tube was determined by an electromagnetic gage and the initial value is about 200 m/s [25]. Due to the large difference between D and u_w, the process of collapse can be considered as axially symmetric and corresponding to plane strain condition. The tangent of angle of collapse is given by the ratio between the two velocities: $u_w/D = 0.05$, corresponding to $\alpha = 2.8°$.

The materials to be tested in the TWC can be solid, porous or granular. In order to avoid the effect of high-speed air jet and melting in the central part during the process of the deformation, two tubes made from "soft", localization resistant metals are used to sandwich the cylinder sample. This helps to maintain a controlled process of specimen collapse.

Fig. 2(a) schematically shows the specimen sandwiched between a copper driver tube and a copper stopper tube that is collapsed inwards during the test. The dimensions of the cylindrical specimen, the copper driver and the copper stopper tubes are shown in Fig. 2(b). The internal diameters of copper (D) were selected to produce prescribed and controlled final strain. In some cases a steel rod was placed in the center of assembly to ensure finely tuned intermediate final strains [31,32]. In the sandwich configuration, the sample cylinder was slid between the copper driver and stopper tubes. The clearances between the sample and these tubes generate a reflection wave followed by impact. To avoid this extra wave reflection from the free interface between the stopper and the specimen, a shrink-fitting technique was applied. The outer diameter of the stopper was designed 0.03 mm larger than the inner diameter of the specimen. The stopper tube was shrunk in liquid nitrogen and then fit into the cylindrical specimen. After the shrink fitting, a pre-strained layer was generated due to the residual stress that may change the stress field in the area where shear bands nucleate.

(a) Schematic process of explosion collapse tests with thick-walled cylinder specimen.

(b) Profiles of the thick-walled specimen and assembly with the copper driver and stopper. D were selected as 11.0 mm and 12.5 mm, respectively.
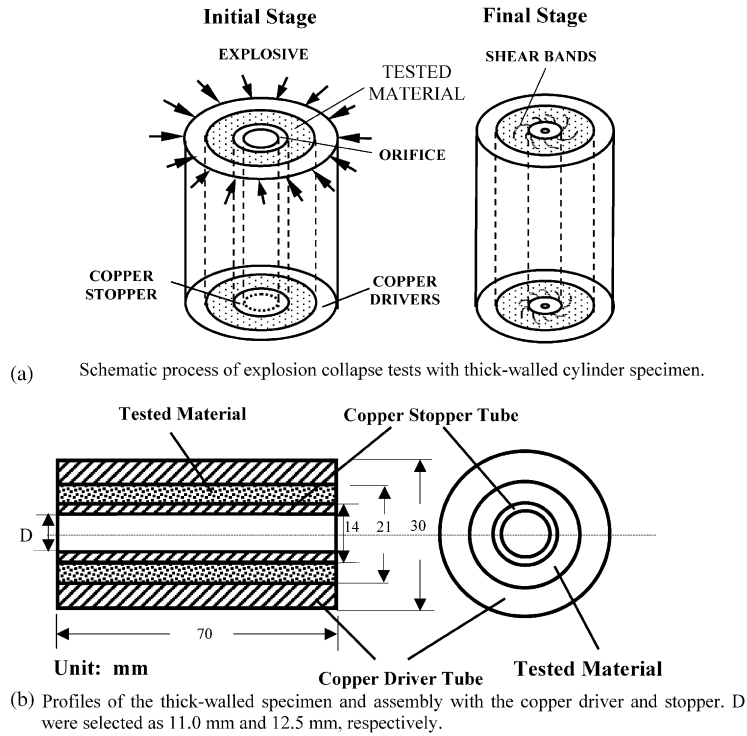
Fig. 2. (a) Principle of collapsed cylinder experiment and (b) dimensions of the TWC assembly.

The collapse of thick-walled cylinder specimen provides an approximate plane strain condition due to the lack of deformation in axial direction. The stress state can be considered as a superposition of a hydrostatic pressure and a pure shear stress due to the axisymmetric geometry. The maximum shear stress and strain occur on the internal surface of the cylindrical specimen, and thus shear bands preferentially initiate there. An effective strain, ε_{ef}, at any point (assuming cylindrical symmetry) is

$$\varepsilon_{ef} = \frac{2}{\sqrt{3}} \varepsilon_{rr} = \frac{2}{\sqrt{3}} \ln\left(\frac{r_0}{r_f}\right), \quad r_f = \sqrt{R_{i0}^2 - R_{f0}^2 + r_0^2}, \tag{1}$$

where r_0, r_f are the initial and final radii of a reference point, R_{i0} and R_{f0} are the initial and final radii of the cavity surface (Fig. 2a). Based on this equation, r_f can be calculated when r_0, R_{f0}, and R_f are measured. It should be mentioned that the effective strain at each point can be determined if the initial geometry is not distorted by the pattern of shear bands. In the case of severe distortion of the geometry in the inside surface, the estimate of global strains can be based on the outside diameter of sample instead of R_{i0} and R_{f0}. After each experiment, the collapsed cylinders were sectioned, ground and polished. The lengths of shear bands, the edge displacements, the average radius of final internal boundary were measured. Based on the number of distinguishable shear bands, n_0, the average spacing

between them is

$$L = \frac{2\pi R_{f0}}{n_0 \sqrt{2}},$$ (2)

where n_0 is the number of shear bands at the internal boundary of the cylinder. In the consideration of geometrical effect, the measured spacing were revised to subtract the geometrical part, reflecting a fact that shear bands initiate at a radius larger than final radius of cavity. The details are discussed in [32].

2.2. Study of multiple shear bands

Multiple shear bands in stainless steel were investigated. Both the as-received and annealed samples were examined for the spacing of shear bands. The 304L stainless-steel bar annealed at 800°C for 3 h retains the same grain size as the as-received steel. The as-received steel was directly machined into the cylindrical tube and the copper stopper and driver tubes were slid into the sample tube with a small clearance ($\sim$0.2 mm). The annealed specimens were first machined into the designed tubes and then subjected to a annealing treatment. Shrink fitting was used to assemble the sample and collapsing accessories. The copper stopper and driver tubes were made with a little overgauge and then shrunk in liquid nitrogen to fit into the sample tube.

(a) As-received Steel $\varepsilon_{ef} = 0.55$ (b) Annealed Steel, $\varepsilon_{ef} = 0.55$

(c) As-received Steel, $\varepsilon_{ef} = 0.92$ (d) Annealed Steel, $\varepsilon_{ef} = 0.92$
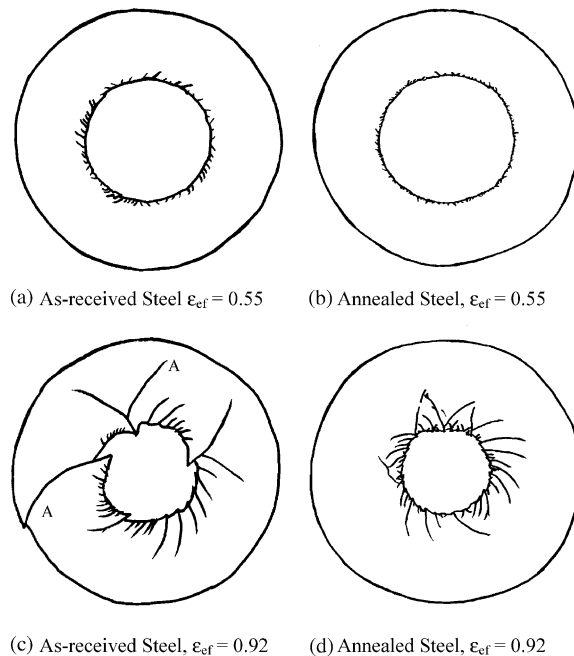
Fig. 3. Shear-band patterns in the thick-walled cylinder specimens at different effective strains; (a) as-received steel, $\varepsilon_{ef} = 0.55$, (b) annealed steel, $\varepsilon_{ef} = 0.55$; (c) as-received steel, $\varepsilon_{ef} = 0.92$; and (d) annealed steel, $\varepsilon_{ef} = 0.92$. Effective strains correspond to the inner surface of the sample.

Figs. 3(a) and (b) show the typical configurations of the shear-band pattern in the as-received and annealed SS 304L at the earlier stage of shear bands. The effective strain at the inner surface of the sample, calculated from Eq. (1), is 0.55. Although the annealed steel reveals a similar pattern as that of the as-received steel, the shear bands in the annealed steel are much shorter than that in the as-received steel. The longest bands are 0.8 mm in the as-received steel and 0.2 mm in the annealed steel. At the later stage (effective strain of 0.92 at the inner surface of the samples), the longest shear band in the annealed steel is only half of that in the as-received steel (Figs. 3(c) and (d)). One band in the as-received steel reached the outer boundary of the cylindrical specimen. The numbers of shear bands in the as-received and the annealed steels at $\varepsilon_{ef} = 0.55$ are 235 and 186, respectively. In comparison with the as-received steel, the annealed SS304 has a lower number of shear bands. The average shear-band spacing for the annealed SS 304L is about 0.15 mm, which is larger than that in the as-received steel (0.12 mm). Fig. 4 shows the comparison of the spectra of shear bands in these two steels at $\varepsilon_{ef} = 0.55$. The abscissa in the plot represents a
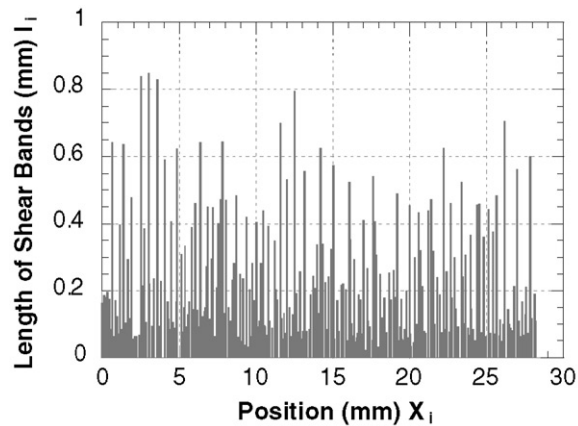
(a)   As-received SS 304
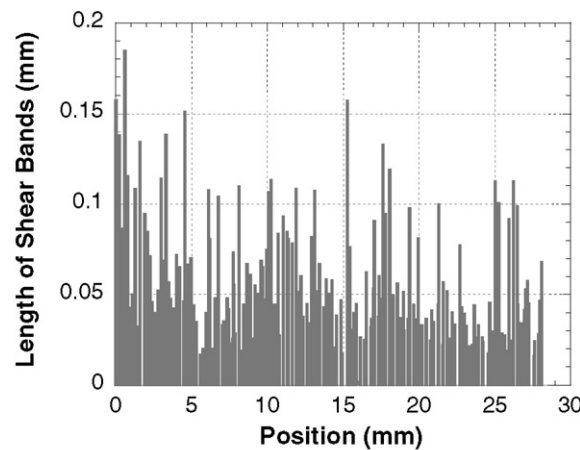
(b)   Annealed SS 304

Fig. 4. Comparison of the shear-band spectra for (a) as-received steel (spacing: 0.12 mm) and (b) annealed steel (spacing: 0.15 mm).
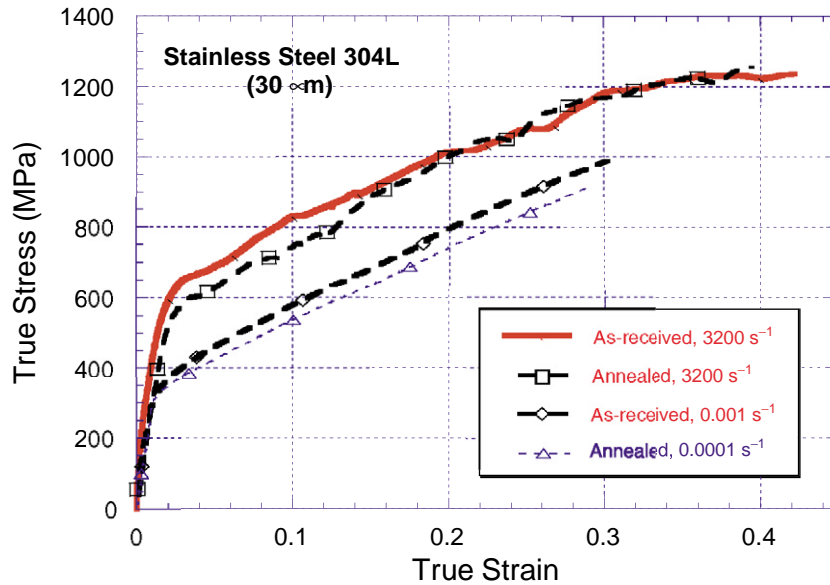
Fig. 5. Quasi-static and dynamic responses of stainless steel 304L in as-received state and annealed state.

circumferential distance from an arbitrarily chosen point. It is clearly seen that the lengths of shear bands at this stage ($\varepsilon_{ef} = 0.55$) in the annealed steel are much smaller than those in the as-received steel. This suggests two possibilities: either the nucleation of shear bands in the annealed steel is more difficult, e.g. the initiation starting at a larger strain, or the propagation speed of shear bands is lower than that in the as-received material.

Annealing at 800°C does not alter the grain size and does not change the mechanical behavior significantly. Fig. 5 shows the comparison of the mechanical responses under quasistatic and dynamic compression for both annealed and as-received 304 steels. Both materials exhibit very similar quasi-static and dynamic responses. This slight difference in mechanical properties should not lead to such a significant difference in the spacing of shear bands. Microstructural observations reveal that the edges of bands at the internal surface of the specimens are much sharper in the as-received steel that in the annealed steel. In the annealed steel, the grains were squeezed out to form a wavy surface with a characteristic wavelength and amplitude on the same order as the grain size, prior to significant shear localization [32]. This implies that the initiation condition of shear bands in these two steels might be different.

The characteristics of the shear bands on the surface of the internal boundary draw our attention to the geometrical and/or loading conditions that may cause these different responses. A series of experiments has been done to verify these effects:

(a) The as-received samples were slide fitted. A clearance existed between the sample and the copper stopper. In the annealed samples, the shrink fitting technique was used and the pre-strained layer existed between sample and the copper stopper.
(b) Another key factor for these steels is the machining effect. The cylindrical specimens in both steels were lathe machined.

3. Role of different effects on the spacing of shear bands

3.1. Machining effect

In the theoretical models [5–7], the nucleation of shear bands is treated without taking into account existing defects. In reality, initiation of a shear band may depend on initial imperfections existing in the nucleation region. In the cylindrical specimen, the imperfect conditions of the internal surface, such as the geometrical defects, non-uniformity of material properties, and pre-strain, may strongly influence the number of nucleation sites, development time and velocity of shear bands. Machining of the samples generates a thin strain-hardened layer that might influence the initiation condition of shear bands. Careful observation of the microstructure at the internal surface of the cylinder of the as-received specimens indicates that a thin layer with heavily deformed grains exists. Fig. 6(a) shows that the thickness of the layer is about 50 μm. Extensive shear deformation due to machining leads to the elongation of the grains close to the surface along the shear direction. The lathe cutter generates such a strain-hardened layer on the surface if
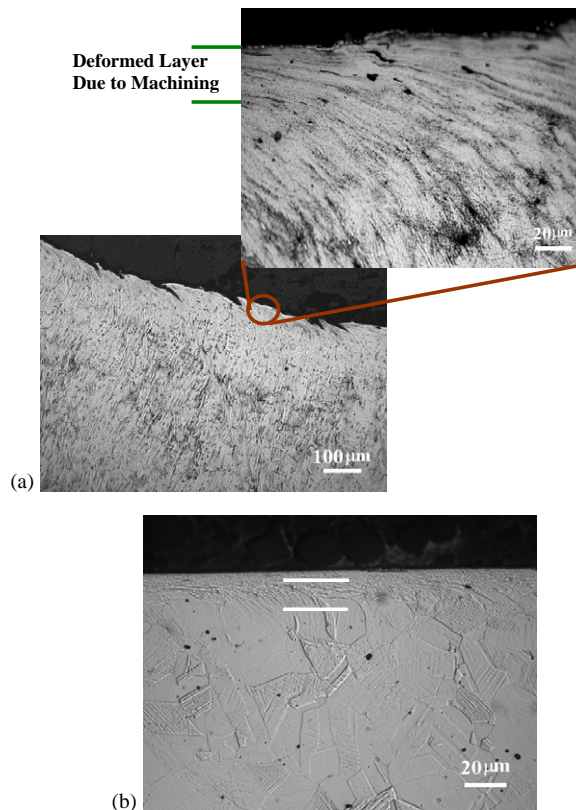
Fig. 6. Pre-deformed layer on the internal boundary of the cylindrical specimen in the as-received stainless steel. Layer generated by the lathe cutter during the machining in (a) the deformed specimen; and (b) the as-received specimen.

the cutting depth and speed exceed certain thresholds. Fig. 6(b) shows such a shear deformed layer at the surface of the sample before the collapsing test.

Experiments were designed to determine the machining effect in the annealed steel. The material was machined into the cylinder sample and then annealed at 800°C for 3 h. This was done to eliminate the work-hardened layer. The as-received rod was also annealed first and then machined into the cylindrical samples. This was done to retain the layer.

The spectrum of shear bands in the specimen machined after annealing at 800°C is given in Fig. 7. The number of shear bands in the steel machined before annealing is 186 at the initial stage (Fig. 4(b)). This number is lower than the steel machined after annealing ($N = 239$). The spacings of shear bands are 0.150 mm for the steel machined before annealing and 0.122 mm for the steel machined after annealing. The latter value is similar to the as-received steel (spacing of 0.116 mm), where a deformed layer was also found. This fact provides solid evidence that the deformed layer introduced from the machining process leads to a different response with respect to initiation of shear localization. Since the unstable deformation heavily depends on the initial perturbation, the change of microstructural characteristics on the initial sites of shear bands, providing a different condition of localization, is one of significant reasons to respond to the spacing variation under two different heat-treated materials. Compared with the spectrum of shear bands in as-received stainless steel in Fig. 4(a), the specimen with 800°C annealing and then machined shows a similar number of shear bands. The as-received material has a band spacing of 0.116 mm, which is a little lower than the spacing for the specimen machined after annealing. The difference between them may be attributed to the contribution of the shrink-fitting effect. Therefore, the machining effect exerts a significant influence on the spacing of initiating shear bands. Thus, additional parameters characterizing material properties in the surface layer should be introduced in the theoretical models predicting shear-band pattern at the nucleation stage.

3.2. Contacting effect

As mentioned in the last section, the existence of small clearances between copper tubes (stopper and driver) and sample tube might also affect the distribution of shear bands. The
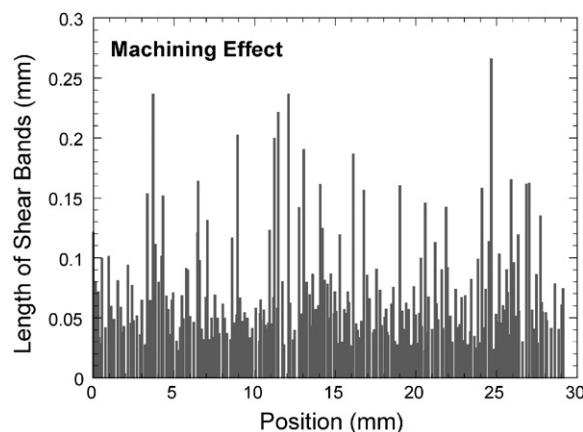
Fig. 7. Shear-band distribution for annealed (800°C/3 h) SS 304 machined after annealing: $N = 239$, and $L = 0.122$.

different sequence of stress waves that are produced at the surfaces of these clearances, therefore, provide a different loading process.

Fig. 8 shows the interface conditions for both the shrink-fitting and non-shrink-fitting cases at the cross-sectional plane of the cylinder. In the non-shrink-fitting case (Fig. 8(a)), a clearance between cylindrical specimen and the copper stopper is required for sliding assembly. When the radial shock wave reaches the specimen, it is reflected at this boundary, resulting in a new shock at impact. Shrink fitting was introduced to remove the clearance in Fig. 8(b). The fitting was completed through the thermal expansion of the inner copper tube. It might introduce a pre-strained layer, but in most of cases the stress keeps in elastic range.

The shear-band distribution in the as-received steel with shrink fitting is shown in Fig. 9. The distribution and spatial pattern in the steel with shrink fitting can be compared with the steel without shrink fitting in Fig. 4(a). The number of shear bands in the shrink-fitted specimen is 249 and is quite similar to that without shrink fitting ($N = 235$) at the same effective strain ($\varepsilon_{ef} = 0.55$). Shear bands at early stage without shrink fitting grow much longer ($l_{MAX} = 0.97$ mm) than in the steel with shrink fitting ($l_{MAX} = 0.29$ mm). However, the spacings of shear bands are almost the same: $L = 0.116$ mm for the steel without fitting and $L = 0.111$ mm for that with fitting. This result indicates that the shrink fitting certainly affects the development of shear bands but does not change their distribution significantly. Actually, the shrink fitting introduced residual stress into the cylindrical specimen. The pre-strain inside the sample is only elastic or at most initially plastic, while the shear localization occurs at large plastic deformation (at the later stage of collapse process). The residual stresses may change the nucleation time of localization and influence the growth speeds of the bands. Distributed uniformly along the tangent direction of the cylinder, the residual stresses cannot affect existing and newly created nucleation sites that control the final spacing of bands.

The clearances are closed at the very beginning of the collapse process and the corresponding strain is far below the critical strain for nucleation of shear bands. The pre-strained layer might result in a little shift of nucleation of shear bands to an earlier time. The shrink fitting removes the delay of wave loading due to the gap and assists to start the nucleation of shear bands earlier.
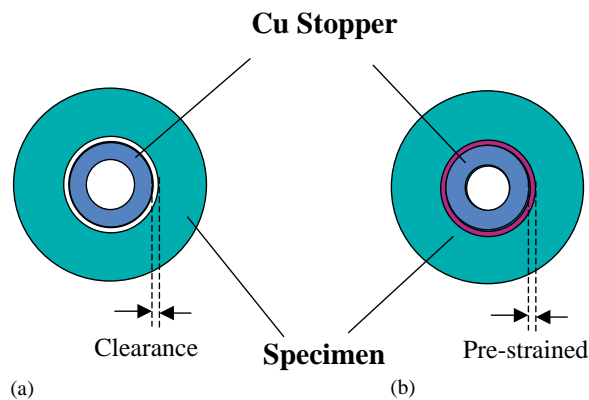
Fig. 8. Contact conditions between the cylindrical specimen and the copper stopper tube for (a) the slide fitting and (b) the shrink fitting.
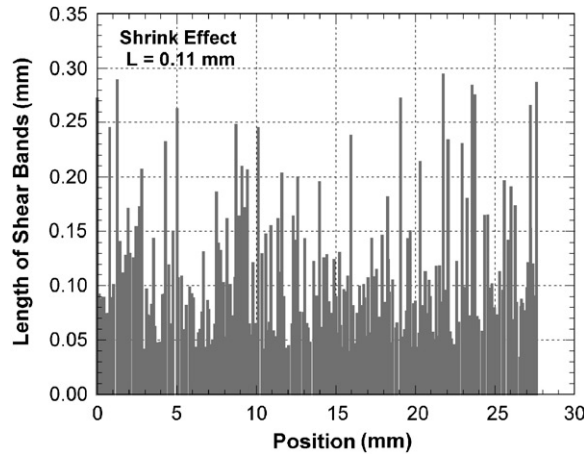
Fig. 9. Shrink-fitting effect on the shear-band spacing. Spacing of shear bands is $L = 0.111$ mm, which is close to $L = 0.116$ mm for non-shrunk specimen.

Therefore, the shrink fitting effect does not influence shear-band spacing, but it changes the process of shear-band development.

3.3. Shear-band distribution along the cylinder specimen

The collapsed cylinder technique is normally considered as a uniform radial compressive process of the cylindrical specimen under a plane strain state. In the real setup of the explosion test, the deformation starts at the top of the cylinder and then propagates along the axis of the cylinder specimen [31,32]. We should mention that a magnetically driven modification of the TWC test, which avoids this effect of explosively driven test, was successfully implemented [33]. The deformation evolution inside the material depends on both the inward driving velocity of the cylinder and the propagation speed of the detonation front. It is important to establish whether the distribution of shear bands can maintain the same pattern along the cylinder ensure the equivalence of the samples sectioned at different heights of the cylinder. In addition, it is important to establish whether the distribution is independent of the boundary conditions at the end parts.

In normal samples (length of 70 mm) the shear-band pattern was usually analyzed in the middle cross-section. A special specimen with longer axial dimension was prepared to examine the longitudinal distribution of shear bands. The radial dimensions are the same as the normal specimens but the length of the specimen was increased from the normal length (70 mm) to 150 mm. After the explosion, the specimen was sectioned into five pieces with a length of about 30 mm as shown in Fig. 10. On each of the four cutting surfaces, a thin piece of sample was sliced. Since the detonation initiated from the top of the specimen, the four samples, taken from upper top to the end, were numbered as SS72, SS73, SS74, and SS75. Each piece was examined for the distribution of shear bands.

The spectra of shear bands in the four samples are shown in Fig. 11. The numbers of shear bands in these samples are 260, 265, 264, and 257. It is clear that all these numbers are at the same
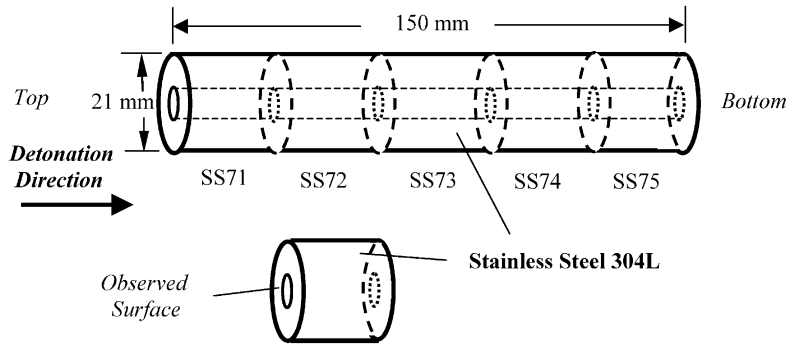
Fig. 10. Selection of the samples along a long cylindrical specimen to determine the repeatability of shear-band patterns at different locations along the bar.
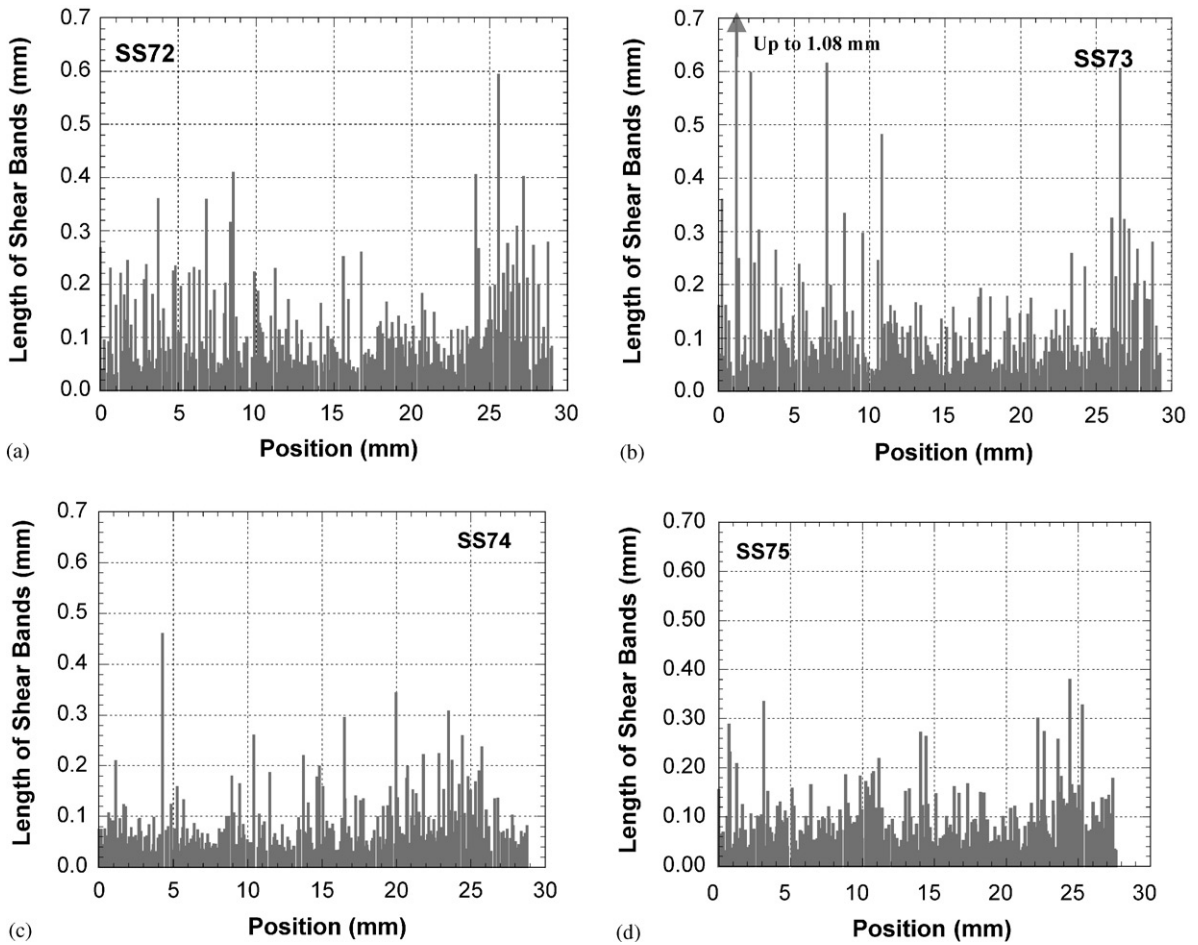
Fig. 11. Spectra of shear-band distribution along a long cylindrical specimen. The sectioned samples list from the top to the bottom shown in (a) SS72–(d) SS75.

level and represent a state of shear independent of the boundary conditions at the ends. The corresponding spacings are 0.112, 0.111, 0.110, and 0.108 mm, respectively. Thus, it can be concluded that the spacing is not influenced by the position of the sectioned sample. Compared with the shear band spectrum in Fig. 4(a), from the middle cross-section of a specimen with normal length, the distribution of shear bands in the middle section of the long specimen (Sample SS73) has a similar maximum length. The spacings in both cases are almost the same: 0.111 mm for the long specimen and 0.116 mm for the regular specimen, respectively. This provides additional evidence that the TWC technique with normal size samples gives a stable, repeatable, and reliable method for studying shear-band patterning.

The parameters of the collective behavior of shear bands (like their number and average spacing) are highly repeatable and usually two or three tests were conducted under identical conditions. The question of reproducibility of shear-band pattern was addressed in an earlier paper [29]. Three identical tests at two strains corresponding to the initiation and well-developed pattern of shear bands in titanium were carried out. The results from the different tests showed excellent reproducibility.

However, from the comparison of the spectra of bands in Figs. 11(a)–(d), it is clear that the development of shear bands along the longitudinal direction is not uniform. The average band length of the sample at the upper top of the cylinder is higher than at the bottom. The sample close to the middle of the long cylinder exhibits a group of longer bands than those at both ends. Fig. 12 shows the distribution of the average length and the maximum length of shear bands along the cylinder specimen. The shadowed bar along the X-axis shows the longitudinal position of the cylindrical specimen. The shear bands in the middle section observably develop faster than in other sections. Strictly speaking, the deformation process is not an ideal plane strain state at both ends. Only the middle section retains a state much closer to plane strain. On the setup, two steel caps were attached on the both ends to fix the tube and to avoid longitudinal damage. These caps may add a certain constraint to alleviate radial collapsed deformation, for example, due to the
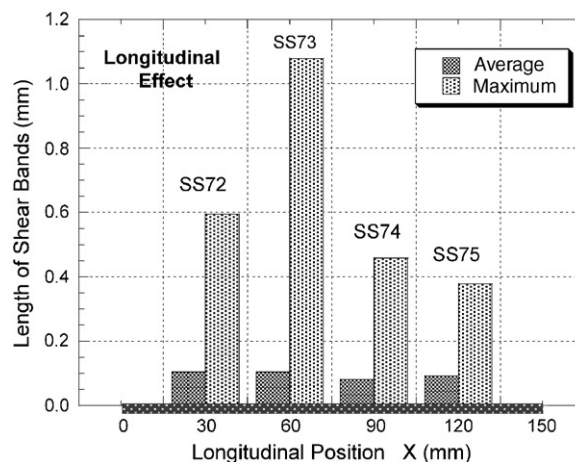
Fig. 12. Distributions of the maximum and the average length of shear bands along the long specimen. Note that the development of shear bands along the bar is not uniform.

friction. Also, the time history of the pressure produced by the detonation products at the end parts of the sample may be slightly different from that in the middle part.

4. Spatial structure of shear bands in the cylinder specimen

The path of shear bands on the sectioned cylinder specimen follows approximately spiral curves. The spatial structure of the shear bands in the collapsed cylinder specimen is a very interesting topic. The intuitional estimation of a band structure in space is a surface with varying curvature. There are very few studies that have discussed the spatial structure of shear bands, either theoretically or experimentally. Meyers and Wang [34] studied shock consolidation of powders in cylindrical configuration and found that helicoidal cracks were produced by compressive shear instability. The loading method in their setup was exactly the same as in collapsed cylinder technique. Fig. 13(a) shows the pattern of helicoidal cracks in the body of a cylinder. They indicated that the helicoidal cracks follow the path of the maximum shear stress. The helicoidal surface intersected the axis direction with 45° at the lateral surface of the cylinder (see Fig. 13(b)).

In the current study, the cylindrical specimen was cut into two pieces along the longitudinal direction. The surfaces from both the tested material and the copper stopper pieces were examined to trace the spatial structure of shear bands. Fig. 14 is an overview of an internal surface of the steel cylinder with relief caused by shear-band patterns. The larger edges of shear band steps left their vertical traces on the surface. Markers show the sections where the larger edges locate. These edges have different directions corresponding to the clockwise or counterclockwise bands, indicated by different directions of markers. The black regions appear to be due to the particles with charging effect under SEM. It is clear that all edges of shear bands are parallel to the axial
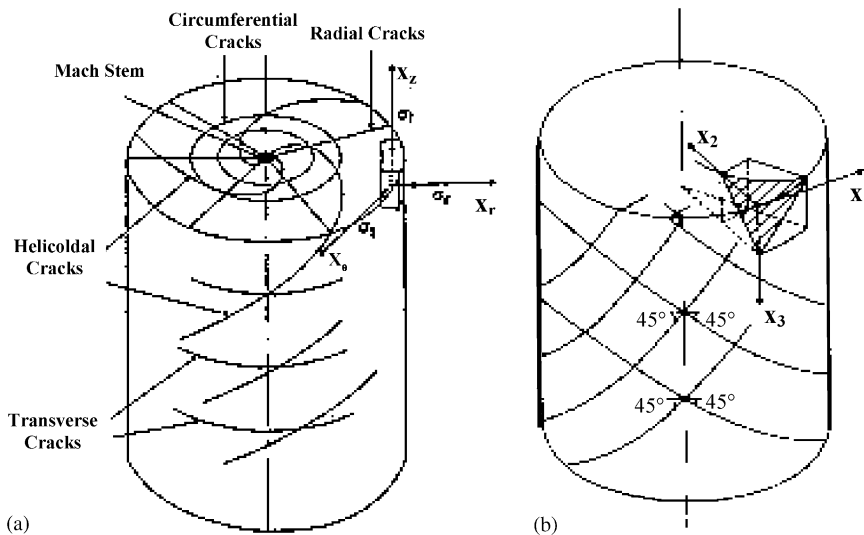
Fig. 13. Predicted paths of unstable deformation in the densified cylinder specimen from [34]. Note that helicoidal surface intersects the cylinder wall with 45° to the axis direction.
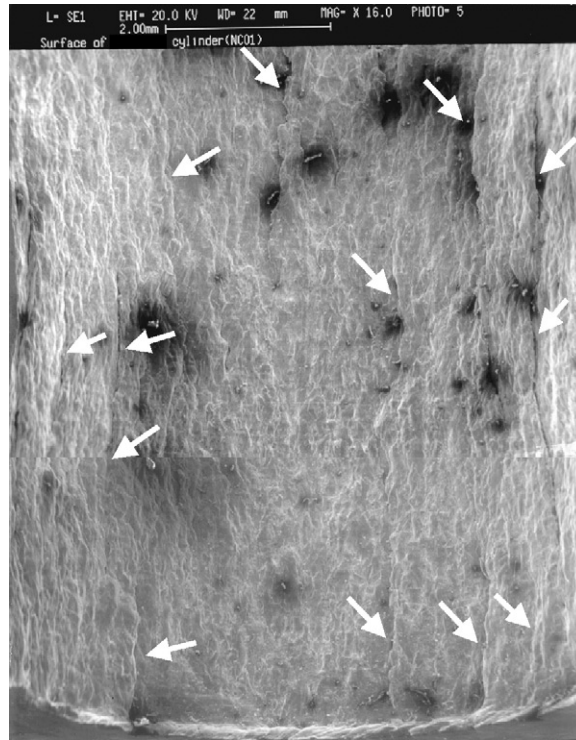
Fig. 14. Overview of the internal surface of the collapsed cylinder in stainless steel. Markers show the locations of the deeper edges that correspond to the long shear bands.
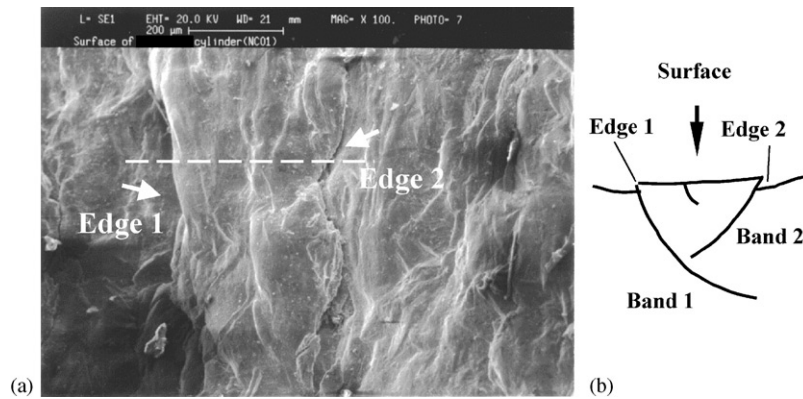
Fig. 15. Reverse deep edges associated with two long shear bands; (a) edge traces on the internal surface of the cylinder and (b) corresponding sectional view of shear bands.

direction of the cylindrical sample. But the amplitudes (lengths) of the edges change along the axial direction of the cylinder.

Fig. 15(a) shows two edges that represent two shear bands in reverse growth direction. They may intersect each other underneath the surface of the cylinder. The surface configuration of
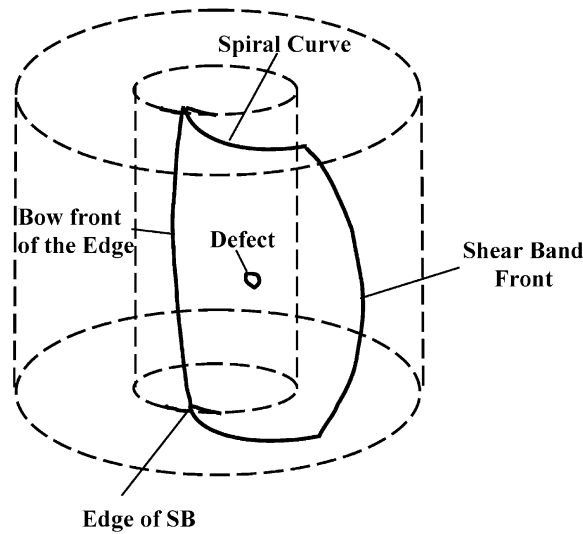
Fig. 16. Spatial structure of a shear band in the collapsed cylindrical specimen.

shear bands is related to the cross-sectional view in Fig. 15(b), which is frequently observed in the internal boundary of collapsed cylinder. All white vertical lines with different lengths correspond to folds of edges of shear bands. It is noticed that the deep edge of a band on the left is quite straight while the right one shows a wavy front (see markers in Fig. 15(a)). This suggests that the localized deformation inside the cylinder, on the scale of the grain size, is not uniform and the length of edges may vary. Actually, recalling the edge pattern in Fig. 14, we can find that several deeper edges appear on the surface. Each of these edges exists on a certain section with a length of 1–2 mm. Both ends of such deeper edges merge into the normally fine edges. This suggests that the edge of the bands slide out to form a bowing front.

It is proposed that the fronts of shear bands are not uniform and have bow-like fronts, since the lengths of shear bands normally correlate directly with the lengths of their edges. The mechanism of such non-uniform development of bands is schematically explained in Fig. 16. The edge length can be considered as a measure of the length of the shear bands. Adjacent shear band planes may coalesce into each other.

5. Numerical simulation of the collapse process

The collapse of cylindrical specimens during the explosion tests is a process of large plastic deformation. Simulation of this process provides a deeper understanding of the physical condition of multiple shear localization. Numerous numerical studies have been performed to describe the unstable process of localization for a single shear band [35–37]. The simulation of the collapsed process including multiple shear-band pattern is beyond the scope of this research. Only the numerical analysis of collapsing process with uniform plastic deformation, using finite element method (FEM), is presented. This approach does not take into account the decrease of strength due to the formation of the shear-band pattern, and the corresponding results can be considered

as an upper limit for the collapse time. Since the major part of mass is concentrated in the copper driver, which deforms uniformly, the neglecting of shear localization will not change the overall kinetics of collapse. A two-dimensional, multi-material Eulerian hydrocode "RAVEN" was used to predict the deformation behavior of the material under explosion loading. This code, developed by Benson [38], has extensive capabilities for solving dynamic problems in solid mechanics and materials science with an emphasis on micromechanics as well as instability of deformation.

Four kinds of materials were involved in the calculation: (a) the tested materials (stainless steel); (b) copper stopper/driver; (c) the explosive, and (d) the air medium inside the central void and outside the explosive. The deformation was considered as a plane-strain state with axial symmetry. In order to simplify the calculation, only a quarter of the cylinder specimen was simulated. The left and bottom boundaries were simply supported. The materials in radial direction can move along the boundary freely, but the axial deformation was constrained. The cylindrical interfaces between different materials were considered to bond together. The initial geometry of the collapsed cylinder setup is shown in Fig. 17. A 60×60 mesh was selected in the calculated square area. The units of both x and y coordinates in the figure are centimeters. The outside and inside parts are air; the rest parts are explosive, copper driving tube, tested material and copper stopper tube correspondingly, starting from outside.

The Johnson–Cook constitutive equation [39] without failure was used in this simulation to describe the material response. This empirical description of constitutive behavior was determined as below:

$$\sigma_y = [A + B\varepsilon_p^n] \cdot [1 + C \ln \dot{\varepsilon}^*] \cdot [1 - T^{*m}], \tag{3}$$
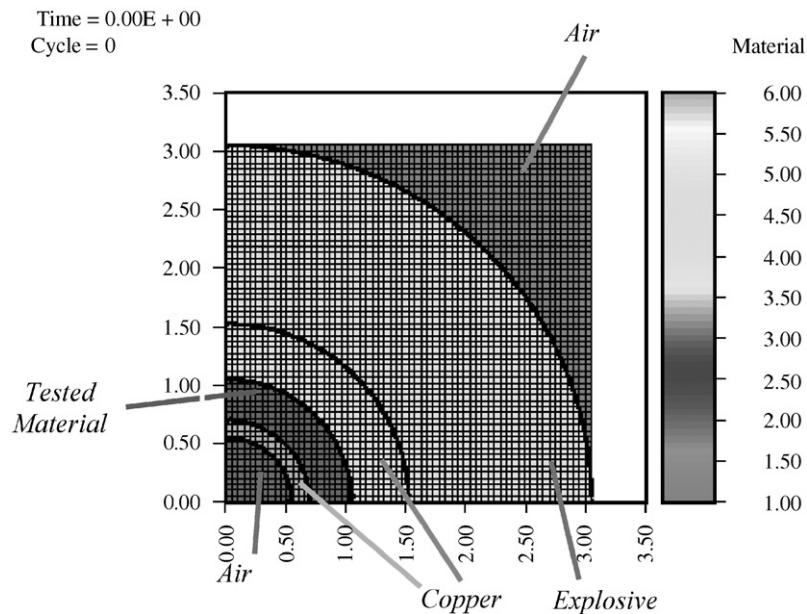
Fig. 17. Geometry of the collapsed cylindrical specimen and the mesh setup. Note that the unit of coordinates is centimeter.

where $\dot{\varepsilon}^*$ and T^* are the normalized strain rate and temperature, respectively, ε_p is the plastic strain. Five material parameters, A, B, C, n, and m, need to be obtained from the properties of the tested material. Using the stress–strain curve of stainless steel under the strain rate of 10^3 s^{-1}, its constitutive response was fitted with the Johnson–Cook equation. The parameters for the tested specimens (AISI 304SS) as well as for the copper are listed in Table 1. The constitutive parameters for OFHC copper were taken from the data of [39]. An explosive with low detonation velocity (4000 m/s) was used in the collapsed technique. A group of reference parameters for the explosive, necessary to complete the simulation, are given in Table 2. It should be mentioned that all calculations here were performed up to the moment when the internal radius of the cavity reaches 0.3 mm, in order to avoid singularity at the center.

The calculations predict (the collapse of the cylinder specimen is a process of stress wave loading) a collapse time of less than 14 µs. The start time is the beginning of loading at the external surface of the sample. Figs. 18(a)–(d) show the progress of the deformed configuration during the explosion test. The radial displacement of the point located at the internal boundary of the cylinder of the tested material is quite small during the first 4 µs. At the time of 14 µs, the hole at the center of the copper stopper was fully closed. This result is quite similar to the experimental result in [26].

A group of points selected to record the history of deformation are used to characterize the behavior of the collapsed cylinder. Fig. 19 shows both the displacement and the velocity of a point on the internal boundary of the stainless-steel cylinder. The deformation starts at about 1.8 µs, which corresponds exactly to the travel duration of the shock wave from the outer boundary (~ 15 mm in radius) to the internal boundary. The cylinder deforms continuously and almost uniformly inward. At 13.5 µs the cylinder completely collapses. The velocity of the internal

Table 1
Parameters of the selected materials for the simulation of collapsed process

Materials	Density (g/cm^3)	Modulus (Mbar)	Shear modulus (Mbar)	Heat capacity (J/g K)	$T_{MELT} - T_{ROOM}$ (K)
OFHC Copper	8.92	1.15	0.440	0.00385×10^{-3}	1058
SS 304L	7.9	2.0	0.775	0.005×10^{-3}	1396
Johnson–Cook equation	$\sigma_y = [A + B\varepsilon_p^n] \cdot [1 + C \ln \dot{\varepsilon}] \cdot [1 - T^{*m}]$				
	A(Mbar)	B(Mbar)	n	C	m
OFHC Copper	0.9×10^{-3}	2.92×10^{-3}	0.31	0.025	1.09
SS 304L	1.1×10^{-3}	15×10^{-3}	0.36	0.014	1

Table 2
Parameters of the explosives

Explosive ammonium nitrite	Detonation velocity U_D(m/s)	Density (g/cm^3)	Gurney energy $\sqrt{2E}$(m/s)	$\gamma = \sqrt{U_D^2/(2E) + 1}$
Low-velocity	4000	0.9	2290	2.17
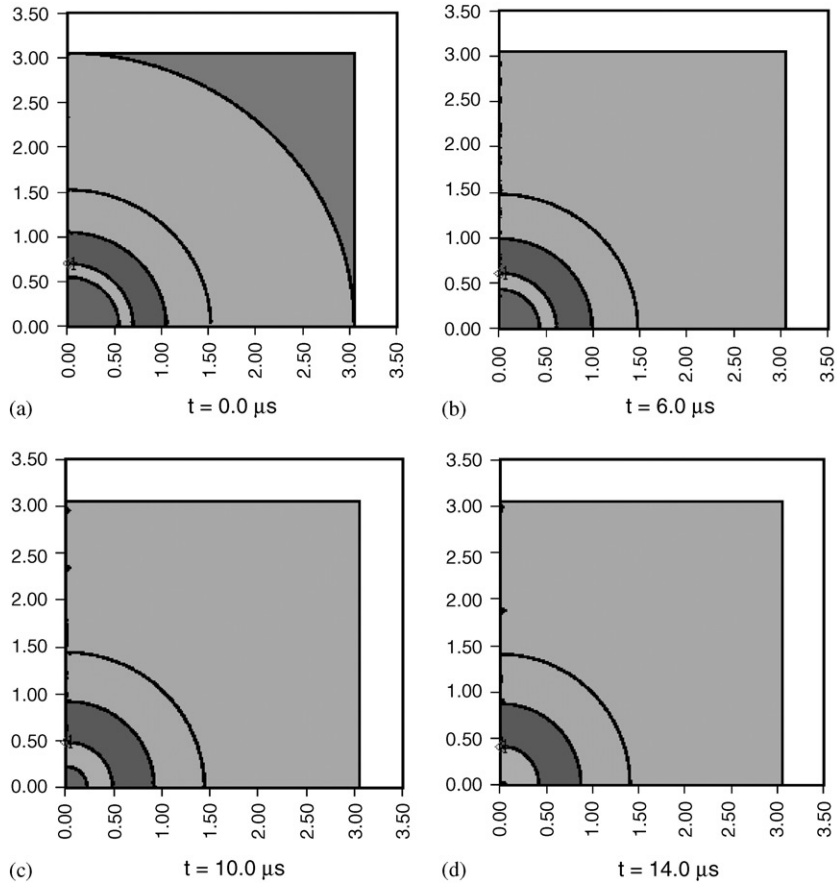
Fig. 18. Evolution of the geometry of the cylindrical specimen during collapse.
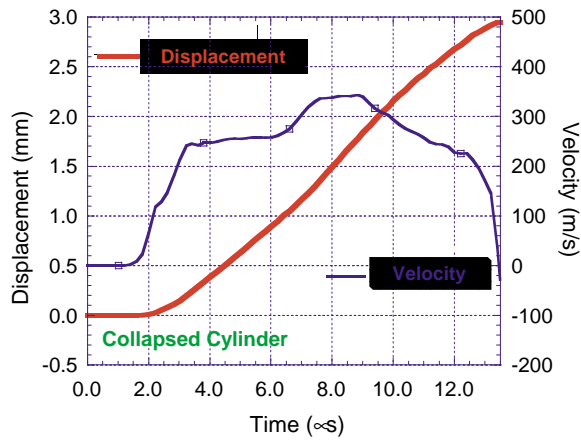
Fig. 19. Displacement and velocity of the point on the internal boundary of the SS 304 cylinder. The thicker and the thinner curves correspond to displacement and velocity, respectively.

boundary varies during the collapse. The velocity increases linearly until it reaches about 250 m/s and then slowly creeps up. There is a step jump at 7.0 μs that results from the second loading waves after the reflected wave arrives at the contact of detonation products and copper driver. A peak of velocity appears at 8–9 μs and has the maximum value of 340 m/s. The velocity drops back to the initial level with higher gradient until the dramatic drop happens *close* (due) to the closure of the central cavity.

The calculation clearly demonstrates that geometrical parameters of TWC method and properties of explosive ensure practically complete dissipation of the kinetic energy at the stage of collapse.

An important parameter is the temperature increase due to a plastic work, which can be approximately estimated from

$$\Delta T = \beta \frac{\sigma \cdot \varepsilon}{c\rho}, \tag{4}$$

where β is the thermal conversion coefficient and can be considered as 1 for adiabatic deformation, and c is the heat capacity.

The temperature increase in stainless steel due to the initial shock wave loading with amplitude 2 GPa and isentropic unloading is about 2 K and can be neglected in the analysis of thermal history.

The internal boundary of the cylinder has the largest plastic strain. The maximum plastic strain there is 0.6, when the hole of cylinder is closed. Fig. 20 gives the temperature variation at the internal boundary of the stainless-steel cylinder, where most of the shear bands initiate. The temperature rises from the ambient temperature (~ 298 K) to about 460 K during the collapse. The calculation shows that the temperature increase corresponding to the start of instability is low (~ 30 K) and does not influence material properties significantly.
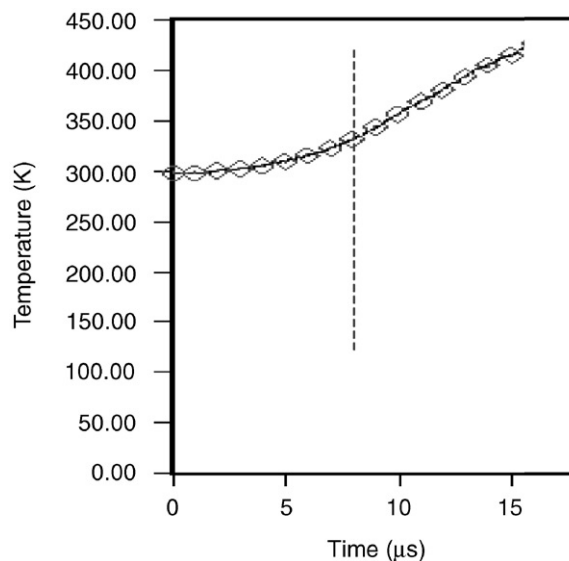
Fig. 20. Temperature history at the internal boundary of the tested cylinder. Note that the dash line shows the starting time of shear localization.

The simulation only provides a uniform, axisymmetric loading configuration. The unstable deformation is not included in the current calculations. Thermally assisted localization would completely change the uniform temperature field. In real experiments, a high-velocity jet is generated in the central part of the collapsed cavity of the copper stopper with partial melting of the central part (0.2 mm).

6. Conclusions

Multiple shear bands in AISI 304 SS were systematically studied by means of the thick-walled cylinder technique. The experimental configuration of this technique is discussed and the limitations are evaluated. The key factors that may influence shear-band distribution and spacing were examined. They include the machining effect, the shrink fitting effect, and annealing effect. The uniformity of longitudinal distribution of shear bands along the cylinder specimen was analyzed. Experimental results indicate that the machined surface at the internal boundary of the cylindrical specimen provide a strain-hardened layer that significantly changes the condition for initiation of shear bands. The specimens with such a layer have a higher density of bands and a smaller spacing than these without work-hardening layers. The interface between sample and copper stopper tube generates either a clearance that interrupted the loading wave at beginning or a pre-strained layer with shrink-fitting technique. This effect does not influence the spacing of shear bands but do change the evolution and development of multiple shear bands, for example, the average length and the nucleation time. The distribution of shear bands along the cylinder was found to be non-uniform. The spacing and average length of shear bands are practically the same but the maximum length of bands in different section varies. The middle section in the cylinder has the fastest growth of shear bands, which consequently have the maximum length. The collapse process of the cylindrical specimen was simulated by using the RAVEN hydrocode. The deformation, temperature, and speed history of the cylinder during the collapse were calculated. The predicted process is in good agreement with previous experimental results.

Acknowledgements

References

[1] Bowden PB. A criterion for inhomogeneous plastic deformation. Philos Mag 1970;22:455–62.
[2] Swallowe GM, Field JE, Horn LA. Measurements of transient high temperatures during the deformation of polymers. J Mater Sci 1986;21:4089–96.
[3] Grady DE. Shock deformation of brittle solids. J Geophys Res 1980;85:913–24.

[4] Grebe HA, Pak H-R, Meyers MA. Adiabatic shear localization in titanium and Ti-6 pct Al-4 pct V alloy. Metall Trans 1985;16A:761–75.

[5] Grady DE, Kipp ME. The growth of unstable thermoplastic shear with application to steady-wave shock compression in solids. J Mech Phys Solids 1987;35:95–119.

[6] Wright TW, Ockendon H. Research note: a scaling law for the effect of inertia on the formation of adiabatic shear bands. Int J Plasticity 1996;12:927–34.

[7] Molinari A. Collective behavior and spacing of adiabatic shear bands. J Mech Phys Solids 1997;45:1551–75.

[8] Marchand A, Duffy J. J Mech Phys Solids 1988;36:261.

[9] Chichili DR, Ramesh KT, Hemker KJ. Acta Mater 1998;46:1025–43.

[10] Meyer LW, Manwaring S. Critical adiabatic shear strength of low alloyed steel under compressive loading. In: Murr LE, Staudhammer KP, Meyers MA, editors. Metallurgical applications of shock-wave and high-strain-rate phenomena in metals. New York: Marcel Dekker, 1986. p. 675–88.

[11] Meyers MA, Subhash G, Kad B, Prasad L. Evolution of microstructure and shear band formation in α-hcp titanium. Mech Mater 1994;17:175–93.

[12] Meyers MA, Andrade U, Chokshi AH. The effect of grain size on the high-strain, high-strain-rate behavior of copper. Metall Mater Trans 1995;26A:2881–93.

[13] Andrade UR, Meyers MA, Vecchio KS, Chokshi AH. Dynamic recrystallization in high-strain, high-strain-rate plastic deformation of copper. Acta Met Mat 1994;42:3183–95.

[14] Backman ME, Finnegan SA. The propagation of adiabatic shear. In: Rohde RW et al., editors. Metallurgical effects at high strain rates. New York: Plenum Press, 1973. p. 531–43.

[15] Meyers MA, Wittman CL. Effect of metallurgical parameters on shear band formation in low-carbon (∼0.20 wt.pct.) steels. Metall Trans 1990;21A:3153–64.

[16] Wittman CL, Meyers MA, Pak H-R. Observation of an adiabatic shear band in AISI 4340 steel by high-voltage transmission electron microscopy. Metall Trans A 1990;21A:707–16.

[17] Meyers MA. Dynamic behavior of materials. New York: Wiley, 1994.

[18] Costin LS, Crisman EE, Hawley RH, Duffy J. On the localization of plastic flow in mild steel tubes under dynamic torsional loading. In: Harding J, editor. Mechanical properties at high rates of strain 1979, Institute of Physics conference series. Bristol: Institut of Physics, vol. 47, 1979. p. 90–110.

[19] Xu YB, Wang ZG, Huang XL, Xing D, Bai YL. Microstructure of shear localization in low carbon ferrite-pearlite steel. Mater Sci Eng 1989;A114:81–7.

[20] Bai Y, Xue Q, Shen L. Characteristics and microstructure in the evolution of shear localization in Ti-6Al-4V alloy. Mech Mater 1994;17:155–64.

[21] Clark EN, Juriaco IP, Mechanics of fragmentation of cylinders. Report AMMRC MS 73-2, Army materials and Mechanics Research Center, Watetown, MA, 1773. p. 311.

[22] Staker MR. On adiabatic shear band determinations by surface observations (of AISI 4340 steel). Scr Metall Mater 1980;14:677–80.

[23] Shockey DA, Erlich DC. Metallurgical influence on shear band activity. In: Meyers MA, Murr LE, editors. Shock waves and high-strain rate phenomena in metals. New York: Plenum Press, 1981. p. 249–61.

[24] Nesterenko VF, Lazaridi AN, Pershin SA. Fiz Goreniya Vzryva 1989;25(4):154–5.

[25] Nesterenko VF, Bondar MP, Ershov IV. In: Schmidt SC et al., editors. High-pressure science and technology—1993. New York: AIP, 1994. p. 1172.

[26] Nesterenko VF, Thick-walled cylinder testing. In: Kuhn H, Medlin D, editors. ASM handbook, vol. 8. Materials Park, OH USA: ASM International, 2000. p. 455–7.

[27] Chen HC, Nesterenko VF, Meyers MA. Shear localization and chemical reaction in Ti–Si and Nb–Si powder mixtures: thermochemical analysis. J Appl Phys 1998;84:1–9.

[28] Nesterenko VF, Meyers MA, Wright TW. Collective behavior of shear bands. In: Murr LE, Staudhammer KP, Meyers MA, editors. Metallurgical and materials applications of shock wave and high-strain rate phenomena. Oxford: Elsevier Science, 1995. p. 397.

[29] Nesterenko VF, Meyers MA, Wright TW. Self-organization in the initiation of adiabatic shear bands. Acta Mater 1998;46:327–40.

[30] Nesterenko VF. Dynamics of heterogeneous materials, New York: Springer, 2001 [Chapter 4].

[31] Xue Q, Nesterenko VF, Meyers MA. Self-organization of shear bands in stainless steel: grain size effects. In: Staudhammer KP, et al., editors. Shock-wave and high-strain-rate phenomena (Proceedings of the EXPLOMET 2000). Oxford, UK: Elsevier, 2000. p. 549–59.

[32] Xue Q, Meyers MA, Nesterenko VF. Self-organization of shear bands in titanium and Ti-6Al-4V alloy. Acta Mater. 2002;50:575–96.

[33] Stokes JL, Nesterenko VF, Shlachter JS, Fulton RD, Indrakanti SS, Gu YB. Comparative behavior of Ti and 304 stainless steel in a magnetically-driven implosion at the Pegasus-II facility. In: Staudhammer KP, Murr LE, Meyers MA, editors. Fundamental issues and applications of shock-wave and high-strain-rate phenomena, (Proceedings of the EXPLOMET' 2000). New York: Elsevier Science Ltd., 2001. p. 585–92.

[34] Meyers MA, Wang SL. An improved method for shock consolidation of powders. Acta Metall Mater 1988;36:925–36.

[35] Litonski J. Plastic flow of a tube under adiabatic torsion. Bull Acad Pol Sci 1977;25:7–14.

[36] Johnson GR. Dynamic analysis of a torsion test specimen including heat conduction and plastic flow. J Eng Mater Tech 1981;103:201–6.

[37] Wright TW, Batra RC. The initiation and growth of adiabatic shear bands. Int J Plasticity 1985;1:202–12.

[38] Benson DJ. Vectorization techniques for explicit arbitrary Lagrangian–Eulerian calculations. Comput. Methods Appl Mech Eng 1992;96:303–28.

[39] Johnson GR, Cook WH. A constitutive model and data for metals subjected to large strain and high strain rate and high temperatures. In: Proceedings of the Seventh International Symposium on Ballistics, Am. Def. Prep. Org., Netherland, 1983.